Three-dimensional Multi-site Random Access Photostimulation (3D-MAP)

Yi Xue[1], Laura Waller[1], Hillel Adesnik[2,*], and Nicolas Pégard[3,4,5,‡]

[1]*Department of Electrical Engineering & Computer Sciences, University of California, Berkeley, CA, USA*
[2]*Department of Molecular & Cell Biology, University of California, Berkeley, CA, USA*
[3]*Department of Applied Physical Sciences, University of North Carolina at Chapel Hill, NC, USA*
[4]*Department of Biomedical Engineering, University of North Carolina at Chapel Hill, NC, USA*
[5]*UNC Neuroscience Center, University of North Carolina at Chapel Hill, NC, USA*
*Corresponding authors : *hadesnik@berkeley.edu, ‡pegard@unc.edu*

Abstract

High precision optical control of neural ensemble activity is essential for understanding brain function and may ultimately revolutionize the treatment of brain disease. Currently only multiphoton holographic optogenetics achieves the requisite spatial resolution for precise neural network control. However, it suffers from critical drawbacks that limit the number of addressable neurons and prevent the development of implantable or wireless devices. Therefore, achieving high-resolution optogenetic control with one-photon activation is essential to catalyze a dramatic leap in spatiotemporally precise multi-site optogenetic technology for research and clinical use. To overcome this challenge, we developed a new light sculpting technique that can synthesize custom illumination patterns in 3D by rapidly projecting structured illumination patterns along with novel computational methods for precise optogenetic control, termed ‘3D-MAP’, for Three-dimensional Multi-site random Access Photostimulation. This technology enables the optogenetic synthesis of complex spatiotemporal sequences of neural activity in the intact brain. As a one-photon photostimulation technology, 3D-MAP can be widely adopted for custom optogenetic applications by the neuroscience research community, and opens the door to scalable, wireless high precision optical brain interfaces.

Introduction

Optogenetics enables rapid and reversible control of neural activity[1,2]. By patterning the illumination light, one can activate or suppress specific neural ensembles in order to map neural circuits, investigate neural dynamics, or attempt to draw links between specific patterns of neural activity and behavior[3-8]. Groups have developed both one-photon[3,4,9-11] and two-photon photostimulation approaches[5, 12-15]. Two-photon photostimulation has the advantage of high spatial resolution for precise neural circuit control and relative immunity to light scattering from tissue, enabling control over deep brain circuits. However, multiphoton absorption is a weak nonlinear light-matter interaction that deposits substantial amounts of heat in brain tissue[16] and requires bulky ultrafast lasers. Those critical drawbacks limit scalability, portability and integration into a broad range of research and future clinical devices.

Within the limits of superficial brain structures or *ex vivo* experiments, one-photon systems have three major advantages. First, one-photon photostimulation can be achieved with much lower power, providing optical control over many more neurons at power levels that are well below thresholds for tissue heating or brain damage. Second, the accessible volume for holographic two-photon photostimulation is limited by the intrinsic characters of the femtosecond pulse laser being used[17], while one-photon systems can be readily scaled to much larger volumes with larger devices, addressing more brain surface and brain regions[18]. Third, unlike two-photon systems, which require physically large and highly energy-consuming lasers, one-photon systems can use small, lightweight diode lasers and compact optoelectronics so that the overall size and

weight of the system can be minimized. These advantages open a path towards future wireless devices that could be directly implanted for behavioral studies in freely moving animals, and integrated into next generation therapeutic brain-machine interfaces.

No one-photon photostimulation technology is yet capable of targeting custom neuron ensembles across a large 3D volume with high spatial resolution. One approach for multi-spot stimulation is to directly project 2D illumination patterns onto the brain with a Digital Micromirror Device (DMD)[3, 10-11]. This widefield illumination scheme has a large Field of View (FOV) and moderate lateral resolution but only modulates light in 2D. Unwanted photostimulation at defocused planes limits its potential for brain interfacing purposes. Another approach, termed Computer Generated Holography (CGH), is to generate 3D distributed foci by phase modulation in Fourier space using a spatial light modulator (SLM)[4, 9]. CGH has high resolution both in the lateral and axial directions, but the FOV is relatively small since 3D resolution is limited by the SLM pixel count and size, and the refresh rate is more than an order of magnitude slower compared to standard DMDs.

To overcome this challenge, we developed 3D multi-site random access photostimulation (3D-MAP), a new approach to generate 3D illumination patterns by modulating light both in the angular domain, (k_x, k_y), with scanning mirrors and in the spatial domain, (x, y), with a DMD. For 3D optogenetic photostimulation, illumination patterns must be optimized to target a photosensitive opsin expressed at the neural soma. The set of light rays needed to generate each (~10μm) spherical target can be

described as a hyperplane within the 4D light field spatio-angular domain, (x, y, k_x, k_y), and these rays can be generated by rapidly sweeping through the appropriate angles of illumination (with the scanning mirrors) while projecting the corresponding amplitude masks of spatial apertures (with the DMD). The accessible volume of 3D-MAP is limited by the size of the DMD and tissue scattering, and the stimulation speed is limited only by the opsin relaxation time and the intrinsic biophysics of the neurons under study. Compared to 2D widefield patterning methods, 3D-MAP retains the advantages of high-throughput and computational efficiency, while extending the addressable space from 2D to 3D. Compared to 3D CGH, where the number of SLM pixels determines the number of degrees-of-freedom (DoF) for volumetric light sculpting, 3D-MAP's number of DoF is much larger - allowing one DMD frame for each unique orientation of the scanning mirrors - because its modulators are both in the spatial and angular domain. 3D-MAP patterns the entire addressable volume at 1.3kHz (the volumetric pattern rate), which exceeds the bandwidth of the majority of neural circuits.

We present the experimental setup and computational methods to synthesize custom 3D illumination patterns and we empirically demonstrate that 3D-MAP achieves very high resolution photostimulation in brain slices and *in vivo* recorded by electrophysiology. We then use 3D-MAP to perform high-throughput synaptic connectivity mapping *in vitro* and *in vivo*, using both single-spot illumination and multi-spot illumination in 3D. These experiments validate 3D-MAP as a one-photon technique to manipulate neural circuits on demand with high spatiotemporal resolution in the intact brain. It can be flexibly used to map neural connectivity at both small and large scales

and correlate causally related complex activity patterns to behavior. In the future 3D-MAP could form the basis of robust, inexpensive, yet highly sophisticated optical brain-machine interfaces.

Results

Optical Design of 3D-MAP

The experimental setup is shown in Figure 1. 3D-MAP uses a DMD to modulate amplitude in real space, (x, y), in combination with scanning mirrors to control the angles of illumination, (k_x, k_y). Both devices are placed at conjugate image planes (Fig. 1a) and time-synchronized. We first compute the light field parameters (x, y, k_x, k_y) of each beam, and display these amplitude masks of spatial aperture with the matching illumination angles one by one (Fig. 1b). The aperture on DMD rotates in a circle as we sweep through each projection angle set by the scanning mirrors. The center of the circle matches the lateral position of the target, and the diameter of the aperture displacement circle, D, determines its axial position. These amplitude masks are computed by ray tracing the perspective views of the target back to the objective's native focal plane. A larger aperture displacement circle diameter corresponds to a target placed further away from the image plane (Fig. 1c). Clockwise and counterclockwise rotations of the projection indicate a target above or below the native focal plane. When the target is at the native focal plane (z=0), the diameter D is zero and we simply turn on the pixel corresponding to the desired position. To simultaneously activate multiple neurons, we generate a multi-site photostimulation

pattern by superimposing the light field parameters (x, y, k_x, k_y) corresponding to each target (Fig. 1c).

The z-sectioning ability of 3D-MAP can be improved by increasing the number of beam illumination angles that are sequentially projected to generate the focus (Fig. 1d-e). However, more amplitude masks require more on-chip memory space of the DMD. Increasing the number of masks will reduce the projection time of each mask but the total simulation time is the same, because the minimum projection time of the DMD (77μs) is about 52-fold shorter than the stimulation time (4ms, see later sections for details). In all experiments, we decided to overlap the beam from 10 high illumination angles to generate high resolution patterns, since the improvement of z-sectioning ability is moderate with additional illumination angles (Fig. 1e). The refresh rate of DMD is 13kHz, and each 3D volumetric pattern is generated by 10 masks on DMD, so the volumetric pattern rate is 1.3kHz, which is much faster than commercial SLMs (low hundreds of Hertz). Since the characteristic timescale of the microbial opsin (or the calibration camera) is much longer than the duration of individual projection masks, the relevant light sculpting pattern is the time-averaged sum of the intensity of several mutually incoherent masks. In addition, the computing speed of masks in 3D-MAP is based on ray tracing and can be calculated much faster than in CGH[19-20]. 3D-MAP is a new method to sculpt light in 3D and enable new real time applications such as mapping neural circuits (see below).

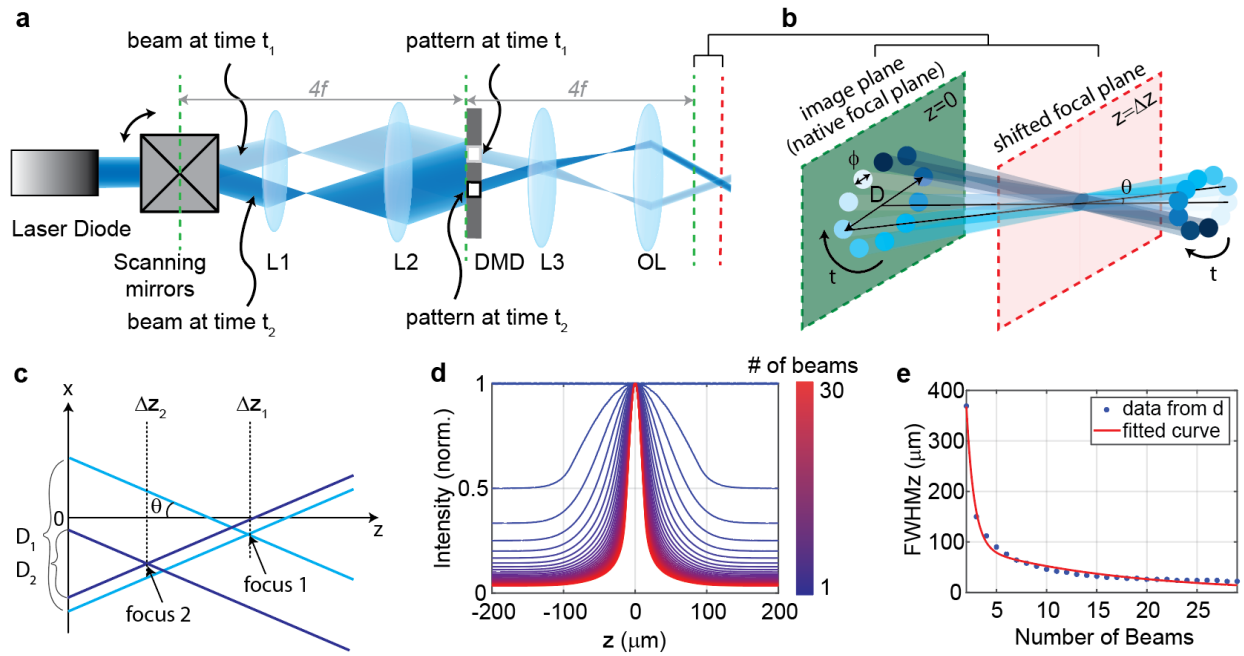

Fig. 1: Experimental setup for Three-dimensional random Access Photostimulation (3D-MAP). (a) A collimated laser beam illuminates the surface of a DMD with a custom illumination angle set by a pair of orthogonal scanning mirrors. The DMD is synchronized with the scanning mirrors to project the corresponding 2D amplitude mask of spatial aperture along the given illumination angle. (b) Detailed view of the overlapping amplitude masks and illumination angles at the conjugate image plane (green) and how synchronized illumination angles and amplitude masks can generate a focus at the shifted focal plane (red). Circular patterns labeled by different colors are spatial apertures projected at different times. The position illuminated by all beams while sweeping through each illumination angle forms a focus at the shifted focal plane (Δz away from the native focal plane at z=0). ϕ is the diameter of the beam. D is the diameter of the sweeping trace. θ is the illumination angle. (c) Multiple foci can be generated simultaneously and at various depths by simple superposition of their perspective projection along each illumination angle. (d) Simulated maximum intensity profile along the z-axis for an increasing number of overlapping beams shows the improvement of 3D-MAP depth sectioning ability. (e) Full width at half maximum (FWHM) of the illumination patterns in (d). The case of one beam is excluded because it has no z-sectioning ability.

Optical Characterization of 3D-MAP

3D-MAP can stimulate multiple targets across a large FOV at very high spatiotemporal resolution. To quantify the spatial resolution of 3D-MAP, we turned on one pixel of the DMD (acting as a point source) and measured the 3D optical point-spread-function (PSF) by imaging a thin fluorescent film on a microscope slide at many depth planes (Fig. 2a-c). The full-width-half-maximums (FWHMs) of the resulting 3D PSF indicate a

spatial resolution of 5x5x18μm^3. We also demonstrated the ability to simultaneously generate 25 foci at custom (x, y, z) locations in a 744x744x400 μm^3 volume (Fig. 2d), with more examples of multi-spot generation in Fig. S1. The temporal resolution of 3D-MAP is 77μs, limited by the maximum refresh rate of the DMD (13kHz). The maximum volumetric pattern rate is 1.3kHz because we need to project 10 masks for each volumetric pattern.

We next evaluated the influence of tissue scattering on focusing capabilities with 3D-MAP by measuring the size of a target after propagating through acute brain slices (brain slices that are kept vital *in vitro* for hours) of increasing thickness on top of the thin fluorescent film (Fig. 2e). We generated a focused target by turning on a 10-pixel radius aperture on the DMD (8μm in diameter at the native focal plane) to produce an illumination volume approximately matching the typical dimensions of a neuronal soma in the cortex. We compared scattering for both blue (473nm) and red (635nm) excitation light. Without the brain slice, the size of the focus was 11.7x11.7x42μm^3 (blue) and 10.4x10.4x50.7μm^3 (red). When generating the focus through 50μm, 100μm and 150μm thick brain slices, the size of the focus spot with blue light increased by 8%, 75%, and 269%, and the size of the focus spot by red light increased by 67%, 107%, and 114%, respectively. Even though the resolution degrades as the brain slice becomes thicker, the effective optical resolution of 3D-MAP is on the order of a single or very small cluster of neurons. Red light suffers less from tissue scattering than blue light. Thus, 3D-MAP should be able to stimulate neurons in brain slices or superficial layers *in vivo* at high spatial resolution.

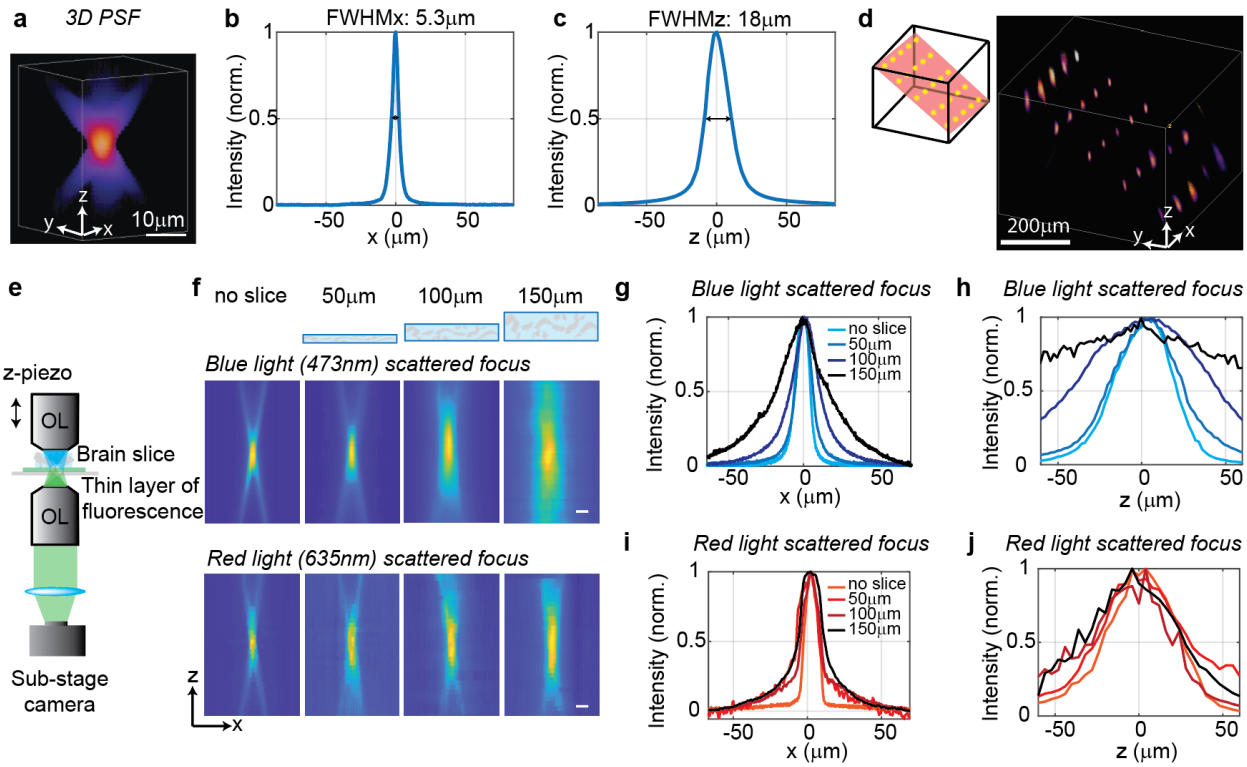

Fig. 2: Optical characterization of the spatial resolution of 3D-MAP with and without scattering. (a) Experimentally measured 3D optical PSF (1-pixel aperture on DMD) built up from slice images of a thin, uniform fluorescent calibration slide recorded at different depths using a sub-stage camera. (b) The PSF's lateral cross-section (x-axis) has a full-width-half-maximum (FWHM) of 5.3μm. (c) The PSF axial cross-section (z-axis) has a FWHM of 18μm. (d) Left: we simultaneously generated 25 foci spanning across a large volume. Right, experimental measurement of the corresponding 3D fluorescence distribution. (e) Schematic diagram of the sub-stage microscope assembly for 3D pattern measurement. To characterize the effects of tissue scattering we experimentally measured foci generated by a 10-pixel aperture on DMD through brain slices of different thickness (0-150μm) using an inverted microscope. (f) XZ cross-section of the scattered PSF, measured by blue and red light stimulation respectively. (g) Under blue light illumination, the FWHM along the x-axis for increased amounts of scattering is 11.7μm, 12.2μm, 19.7μm, and 29.0μm. (h) Under blue light illumination, the FWHM along the z-axis is 42μm, 46μm, 76μm and 122μm. (i) Under red light illumination, the FWHM along the x-axis for increased amounts of scattering is 10.4μm, 19.3μm, 26.7μm, and 29.6μm. (j) Under red light illumination, the FWHM along the z-axis for increased amounts of scattering is 50.7μm, 75.4μm, 79.7μm, and 73.1μm.

3D-MAP Photostimulation with very high spatial resolution in brain tissue

We next quantified the physiological spatial resolution as measured by the physiological point spread function (PPSF) of 3D-MAP by stimulating neurons in acute mouse brain slices and *in vivo*. We made whole cell patch clamp recordings from L2/3 excitatory

neurons expressing the potent, soma-targeted optogenetic protein ChroME[15] (see Methods). The PPSF records the photocurrent response as a function of the displacement between the targeted focus and the patched cell[14]. Since 3D-MAP is able to calculate and project patterns much faster than CGH, we measured the volumetric PPSF by recording the photocurrent response from 2,541 targeted locations (a 11x11x21 pixels grid) in 2-5 minutes, limited only by opsin kinetics (4ms photostimulation followed by 8-40ms relaxation time at each pixel, varying by opsin). The PPSF measurements show that 3D-MAP provides near single-cell resolution photostimulation *in vitro* (lateral full width at half maximum (FWHM), 29±0.8μm; axial FWHM, 44±1.6μm, 9 cells, Fig. 3a-c) , only approximately two-fold worse than prior measurements with multiphoton optogenetics[14-15,21.] We also measured the spiking probability of neurons in acute brain slices and in living mice along the lateral and axial dimensions in order to quantify the physiological resolution of 3D-MAP for suprathreshold neuronal activation. While patching the neuron, we digitally displaced the target generated by 3D-MAP along the x-axis and z-axis. The result also demonstrates very high spatial resolution under these conditions (Fig. 3d-e, *in vitro* results, lateral FWHM, 16±2.4μm; axial FWHM, 44±8.9μm, 5 cells; Fig. 3i-j, *in vivo* results, lateral FWHM, 19±3.7μm; axial FWHM, 45±6.1μm, 8 cells). Together, these data validate 3D-MAP as a novel scanless 3D one-photon light sculpting technique for optogenetic stimulation with very high spatiotemporal resolution in the mouse brain.

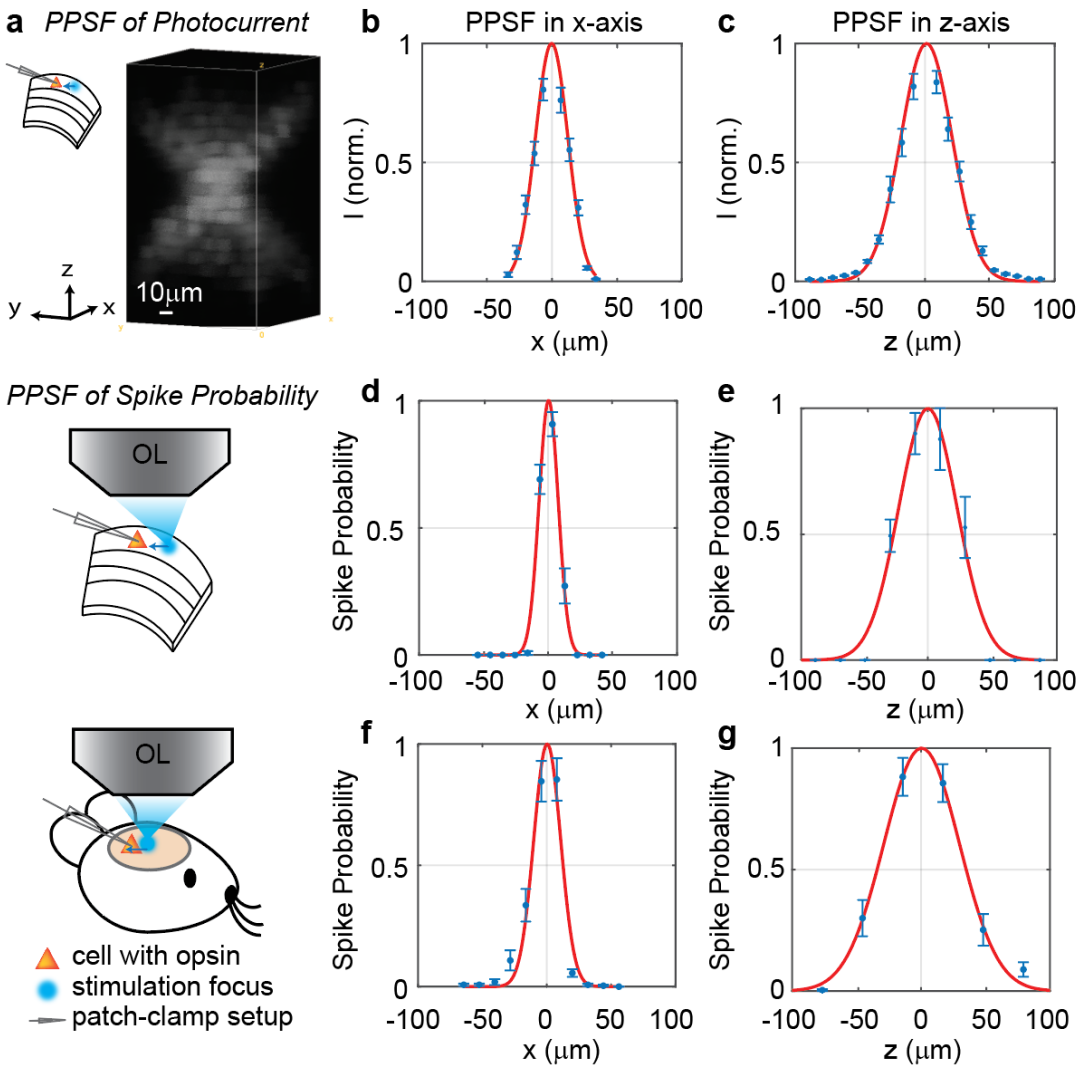

Fig. 3: 3D-MAP provides high spatial resolution photo-activation of neurons *in vitro* and *in vivo*. PPSF, physiological point spread function. (a) Example image of a 3D physiological point spread function (PPSF) measurement *in vitro*. (b-c) Photocurrent resolution (FWHM) is 29±0.8μm laterally, and 44±1.6μm axially (n=9 neurons). (d-e) 3D-MAP evoked spiking resolution in brain slices is 16±2.4μm laterally and 44±8.9μm axially (n=5 neurons). (f-g) 3D-MAP evoked spiking resolution measured *in vivo* is 19±3.7μm laterally and 45±6.1μm axially (n=8 neurons). The data represents the mean ± s.e.m (standard error of the mean) for all plots.

High throughput synaptic connectivity mapping over large volumes with 3D-MAP

In addition to high spatiotemporal resolution and fast computational speed, 3D-MAP is easily scalable and can address large volumes at various stimulation powers. To demonstrate these advantages, we used 3D-MAP to probe synaptic connectivity in 3D (Fig. 4). We expressed ChroME in excitatory neurons of the cortex (see Methods), then

made whole cell voltage clamp recordings from inhibitory interneurons that do not express ChroME under these conditions, to avoid the confounding effect of direct photocurrents in the patched neuron (Fig. 4a). The wide-field fluorescent image (Fig. 4b) shows the excitatory neurons (red) and the patched inhibitory interneuron (green). We first mapped a 800x800μm^2 FOV at low spatial sampling (40μm grid) to identify a sub-region that contained most of the presynaptic neurons (Fig. 4c), and then mapped that sub-region at fine resolution (Fig. 4d) and even higher resolution (Fig. 4e). Due to variable opsin protein expression levels across neurons, as well as variable intrinsic neural excitability, neurons are differentially sensitive to light. By mapping the same sub-region at different power levels, we could take advantage of this fact to help identify putative individual (i.e., 'unitary') sources of presynaptic input (Fig. 4d). Photostimulation generated excitatory postsynaptic currents (EPSCs) at many locations, and importantly, most connectivity maps exhibited spatial clusters like synaptic input maps in space (Fig. 4e). Within each cluster, most of the postsynaptic responses had similar amplitudes and time courses, suggesting they primarily arose from just one or a small number of presynaptic neurons (Fig. 4f-g). We also performed the synaptic connectivity mapping *in vivo* (Fig. S2). These results demonstrate that 3D-MAP is easily scalable and suitable for obtaining extremely high resolution connectivity maps of neural circuits.

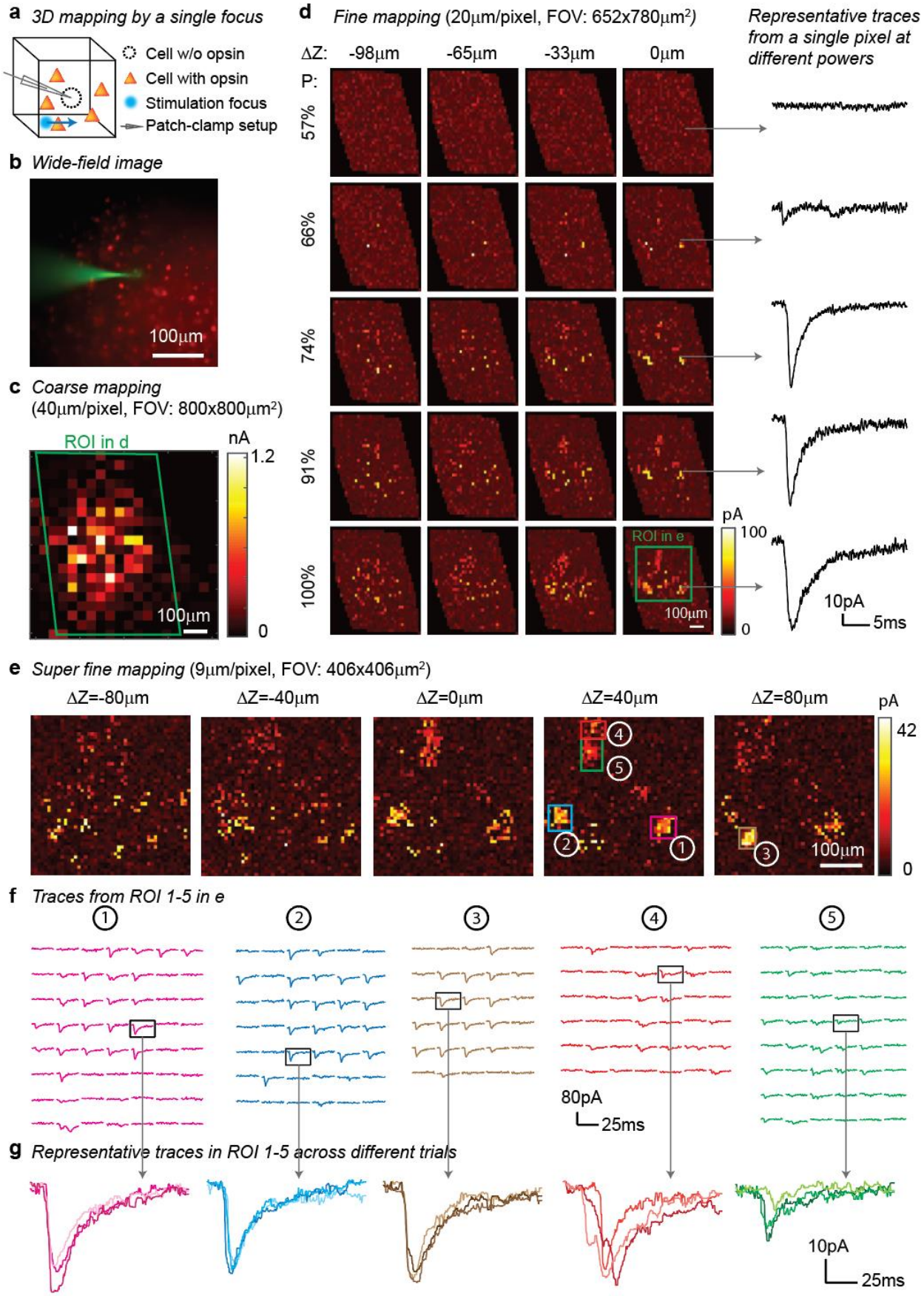
a 3D mapping by a single focus
Cell w/o opsin
Cell with opsin
Stimulation focus
Patch-clamp setup
b Wide-field image
100μm
c Coarse mapping
(40μm/pixel, FOV: 800x800μm²)
ROI in d
nA
1.2
0
100μm
d Fine mapping (20μm/pixel, FOV: 652x780μm²)
Representative traces from a single pixel at different powers
ΔZ: -98μm -65μm -33μm 0μm
P:
57%
66%
74%
91%
100%
ROI in e
100μm
pA
100
0
10pA
5ms
e Super fine mapping (9μm/pixel, FOV: 406x406μm²)
ΔZ=-80μm
ΔZ=-40μm
ΔZ=0μm
ΔZ=40μm
ΔZ=80μm
pA
42
0
100μm
f Traces from ROI 1-5 in e
80pA
25ms
g Representative traces in ROI 1-5 across different trials
10pA
25ms

Fig. 4: 3D Mapping of excitatory synaptic connections with 3D-MAP. (a) Schematic diagram of the experiment. A single focus randomly scans the volume adjacent to the patched interneuron (which does not express opsin), and the readout map reveals the synaptic connections between photo-activated pyramidal neurons and the patched interneuron. (b) Example of widefield image of opsin-expressing pyramidal neurons (red) and the patched interneuron (green). (c) A coarse 2D map in a (800x800μm^2 FOV) at 40μm resolution identifies the sub-region of the brain slice with presynaptic neurons. (d) Mapping the selected region at higher resolution (green box in c). Each row uses the same stimulation laser power (100% power: 145μW) across multiple axial planes, and each column is a map of the same axial plane at different powers. Representative EPSC traces on the right show how synaptic currents at the same photostimulation pixel change as the stimulation power increases, presumably due to recruitment of additional presynaptic neurons. Data are averaged over 5 repetitions. (e) Super-fine resolution mapping of the region of interest (ROI) (green box in d) in 3D at P=90μW. (f) Traces from ROIs 1-5 labeled in e, averaged over 5 repetitions. (g) Representative traces of single trials without averaging from corresponding ROIs in the same color, measured across three different repetitions.

One of the major advantages of 3D-MAP over conventional single point scanning approaches (e.g., with galvo/galvos) is that it has the capacity to stimulate multiple neurons simultaneously distributed anywhere in the addressable volume. Multi-site photostimulation is crucial for perturbing or mapping brain circuits because only the activation of neural populations can drive the sophisticated activity patterns needed to understand network dynamics or behavior. Thus, we next demonstrated that 3D-MAP is able to simultaneously stimulate multiple user-defined targets (Fig. 5). While patching the same inhibitory interneuron as described above (Fig. 5b, the same as Fig. 4e), we first stimulated the 5 presynaptic ROIs one-by-one, and then stimulated subsets of them simultaneously, and finally stimulated all the ROIs together (Fig. 5c). We compared the photocurrent measured by multi-site simultaneous stimulation (Fig. 5d, blue, stimulation of all the ROIs) to the linear sum of individual responses by single stimulation (Fig. 5d, red, the sum of the first row of Fig. 5c) and observed the multi-site stimulation generates greater net input (Fig. 5e, p=0.0488 for 2-5 sites stimulation, two-way analysis of variance (ANOVA)). This example shows that 3D-MAP is able to simultaneously

stimulate multiple targets and also can flexibly adjust the 3D patterns in real time, which is important for online interrogation of neural circuits.

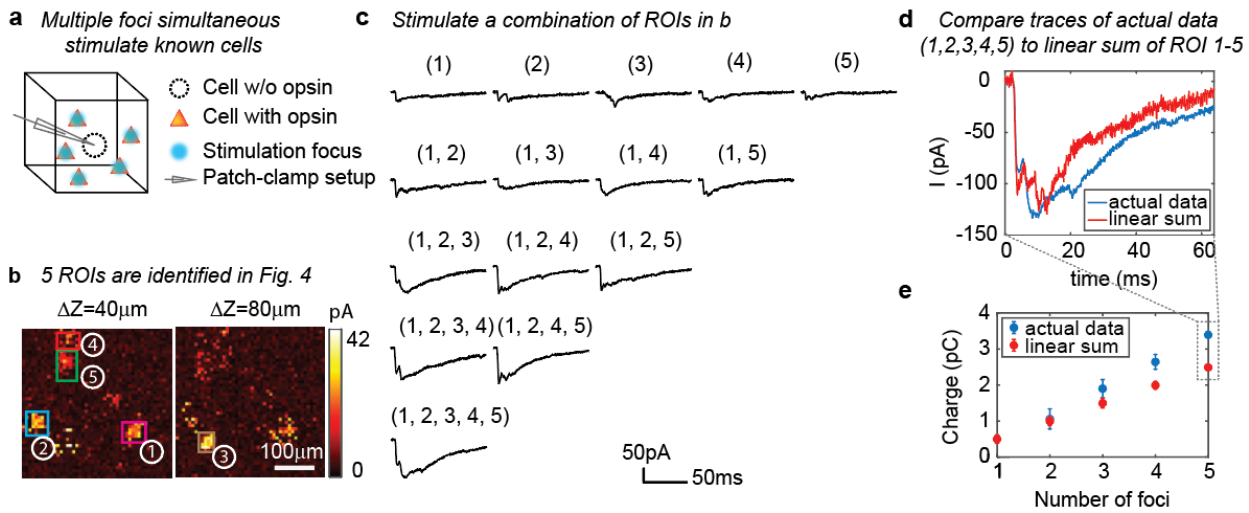

Fig. 5: 3D-MAP is able to stimulate multiple targets simultaneously to explore network dynamics. (a) Schematic diagram of the experiment. (b) The position of 5 ROIs are identified from Fig. 4e. (c) Representative traces for simultaneous stimulation of subsets of the 5 ROIs. Traces are averaged over 4 repetitions. The number(s) above each trace indicate the ROIs that were stimulated to generate the response. (d) Comparison of the actual synaptic response to simultaneous stimulation of ROI 1-5 (blue) to the response calculated by linearly summing the traces when stimulating ROI 1-5 individually (red). The individual response from each ROI is shown in the first row of c. (e) Comparison of the integral of the synaptic current from simultaneous stimulation of multiple connected presynaptic neurons (blue) to the linear sum of the individual stimulation responses (red). The mean and standard deviation of data is calculated from all the k-combinations (number of foci) from the given set of 5 targets. The sample size is $C(5,k), k = 1,2,3,4,5$.

Reconstructing synaptic networks with 3D-MAP via gradient descent

Ultimately, physiological brain mapping approaches must overcome the challenge of temporal throughput to map ever larger regions of brain tissue. We reasoned that mapping neural circuits with multiple foci, rather than a single focus, could scale up the temporal throughput of the system dramatically, since the overall connectivity matrix is remarkably sparse. Instead of randomly shifting a single focus to measure the one-to-one synaptic connections (as in the last section), we used 3D-MAP to stimulate multiple

random voxels simultaneously and reconstructed the spatial map of presynaptic networks via gradient descent. Here, the positions of the simultaneously stimulated voxels were randomly distributed in the 3D volume, unlike co-stimulating known presynaptic ROIs in the last section. In acute brain slices we again patched a GABAergic interneuron under voltage-clamp mode and recorded both EPSCs, and subsequently, inhibitory postsynaptic currents (IPSCs). We projected random sets of foci (five at a time) and repeated this process until all voxels in 3D were stimulated several times (typically 5-10). Since the recorded photocurrents are a combination of responses from multiple sites, we used an optimization algorithm based on gradient descent to reconstruct the map of the synaptic network (see Methods).

Results in Fig. 6 show the excitatory synaptic network map and inhibitory synaptic network map of the same GABAergic interneuron in an 800x800x200μm^3 volume at three different stimulation powers. Multi-site simultaneous stimulation has two key advantages. First, perhaps more importantly, multi-site stimulation engages the activity of spatially distributed ensembles of neurons (rather than single neurons or small local clusters), which may facilitate polysynaptic network activity and engage network level properties of the circuit. Second, it is possible to reconstruct the same mapping results with fewer measurements compared to single-target stimulation based on compressive sensing, assuming the multiple stimulation sites are sparse and the readout signal is a linear combination of the inputs from these sites. The assumption is valid when the multiple voxels for concurrent stimulation are randomly drawn from the volume and the number of these voxels are much smaller than the total voxels in the volume (5 voxels

are randomly drawn from 1600 voxels in our experiment). Since multiple voxels are stimulated at the same time (say N voxels), each voxel needs to be measured N times with different patterns to distinguish the current from each voxel. Under the assumption of sparsity and linearity, we can reconstruct the map of neural networks with less repetitions (Fig. S3, Methods). This feature of 3D-MAP is important to speed up the mapping of a large volume where single-target stimulation of every voxel would take too long.

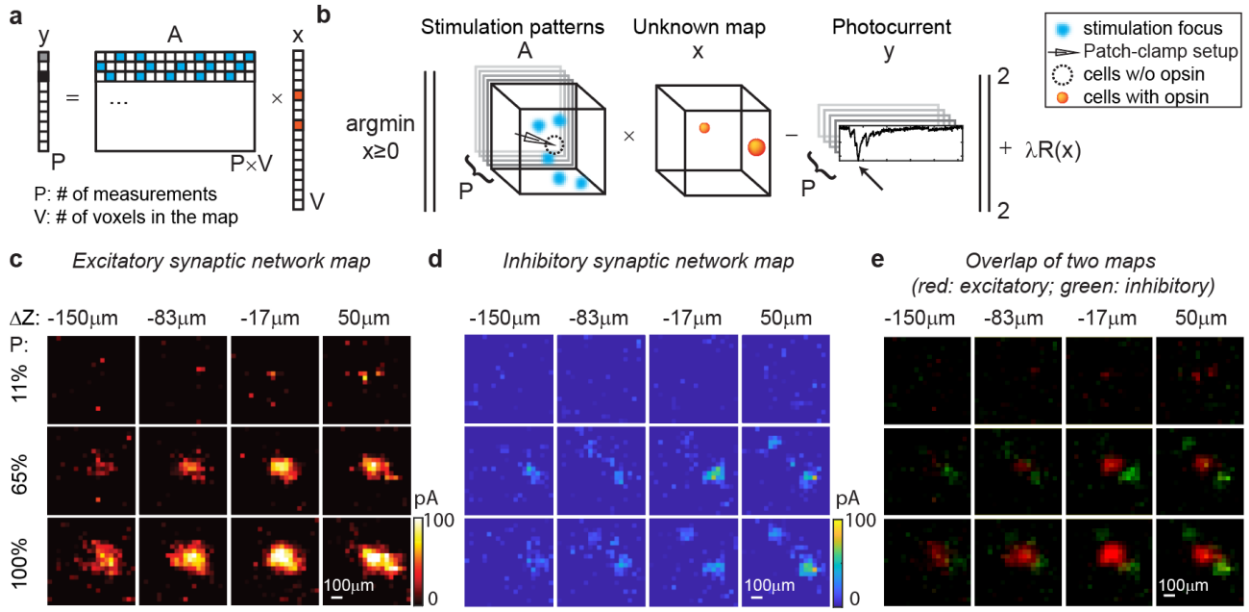

Fig. 6: Mapping of synaptic networks *in vitro* by multi-site simultaneous stimulation and computational reconstruction. (a) Forward model for multi-site simultaneous stimulation. V, the number of voxels in the 3D volume. P, the number of patterns, which are orthogonal to each other. y, peak value of the measured synaptic currents. A is a matrix, where each row represents an illumination pattern, including 5 foci here (blue, N=5). x is a vector of the unknown synaptic networks to be reconstructed. (b) Inverse problem formulation. The aim is to approximate x by minimizing the difference between the peak of measured currents (y) and those expected via the forward model with a regularizer $\lambda R(x)$. The details are in Methods. (c) Excitatory synaptic connection map of a GABAergic interneuron (at [0, 0, 0]). (d) Inhibitory synaptic connection map from the same cell. (e) Overlap of the excitatory map (red) and inhibitory map (green) to show their spatial relationship. Figures in (c-e) are recorded in an 800x800x200μm^3 volume at three different stimulation powers (100% stimulation power is 890μW). The number of simultaneous stimulation foci (N) is five in both cases and the results are average over five repetitions.

Discussion

In this study we demonstrated and validated 3D-MAP, a one-photon technique that enables 3D multi-site random access illumination for high precision optogenetic photostimulation. 3D-MAP combines novel computational and optical advances to offer an extremely powerful and flexible optical brain perturbation system. Unlike prior one-photon approaches that have low spatial resolution, or prior two-photon approaches that are severely limited in their scalability and speed, 3D-MAP achieves high spatial precision at extremely high speeds and in large volumes in the superficial layers of the intact brain. 3D-MAP is the first system to achieve 3D multi-site illumination by simultaneously sculpting the light field in both intensity and angular domains. This makes 3D-MAP far more versatile with many more degrees of freedom than CGH. Therefore, 3D-MAP is able to generate high resolution 3D patterns that CGH cannot synthesize given its limited frequency bandwidth in Fourier space. In addition, 3D-MAP is able to project 3D patterns at much faster speeds than CGH not only because the refresh rate of the DMD is an order of magnitude faster than in an SLM, but also because calculating the light field parameters with ray tracing in 3D-MAP is much faster than calculating phase masks in 3D CGH. The fast patterning rate of 3D-MAP will enable real-time applications such as close-looped optogenetics, that are likely to become increasingly important in both research and clinical applications.

Most importantly, 3D-MAP, unlike two-photon approaches, is perhaps the technology that is best amenable to upscaling to address mesoscale volumes, as well as downscaling into a wireless, miniaturized device. Scaling up could be achieved by conjugating the large format DMD used in this study to a high numerical aperture, low

magnification objective, as used in mesoscopes. Scaling down into a compact implantable device could be achieved by leveraging miniature DMDs (as currently used in commercial pico-projectors) and small visible laser diodes into a miniature microscope technology. Thus, 3D-MAP is poised to become both a widely used tool in basic neuroscience research but could also ultimately form the basis of next generation optical brain neuroprostheses.

Methods

Ethical statement. All animal experiments were performed in accordance with the guidelines and regulations of the Animal Care and Use Committee of the University of California, Berkeley.

Data availability. The datasets generated during and/or analysed during the current study are available from the corresponding author on reasonable request.

Code availability. Custom code used to collect and analyze data is programed in MATLAB. The code has been deposited in Github (https://github.com/Waller-Lab/3D-MAP).

3D-MAP optical setup. The laser sources for optogenetic stimulation are Diode Pumped Solid State (DPSS) laser diodes. One is at 473nm wavelength (MBL-N-473A-1W, Ultralasers, Inc., Canada) and the other at 635nm wavelength (SDL-635-LM-5000T, Shanghai Dream Lasers Technology Co., Ltd., China) for different opsins. The results shown in Fig. 6 are measured under red stimulation, and all the others are stimulated by blue light. The laser source for *in vivo* PPSF (Fig. 3f-g) and wide-field

imaging (Fig. 4b) is a DPSS laser at 589nm wavelength (MGL-W-589-1W, Ultralasers, Inc., Canada). Both current supplies are externally driven by an analog modulation voltage. The laser beams are scanned by a pair of galvo-mirrors (GVS202, Thorlabs, Inc., U.S.), and then the beam size is expanded to fill the DMD (DLP9000X and the controller V4390, ViALUX, Germany) by a 4-f system (f_1=45mm, f_2=150mm). The DMD is mounted on a rotation base in order to maximize the output laser power from 'ON' pixels and minimize the diffraction pattern from DMD pitches. Then the patterned beam passes through a tube lens (f=180mm) and the objective lens (XLUMPlanFL N, 20x, NA 1.0, Olympus) to generate holographic foci. The objective lens is mounted on a motorized z-stage (FG-BOBZ-M, Sutter Instrument, U.S.). A customized dichroic mirror (zt473/589/635rpc-UF2, Chroma, U.S.) is placed before the objective lens to reflect the stimulation laser beams while transmitting fluorescence photons emitted from the sample. The wide-field fluorescence image is recorded by a camera (Prime95B, Teledyne Photometrix, U.S.). Brain samples (acute brain slices and anesthetized mice) are placed on a motorized x-y stage (X040528 and the controller MP-285, Sutter Instrument, U.S.). The 3D pattern (Fig. 2 and Fig. S1) is measured by capturing the fluorescence excitation in a thin fluorescent film on a microscope slide, with a sub-stage objective (XLUMPlanFL N, 20x, NA 1.0, Olympus) coupled to a camera (DCC1545M, Thorlabs, U.S.). The targeted positions in a 3D pattern are stimulated in a random order: two sequential stimulations are separated by a minimum distance calculated by Poisson disc sampling in order to avoid photocurrent accumulation caused by repeat stimulation. Tomographic renderings of the 3D-MAP illumination patterns are obtained by mechanically scanning the sub-stage slice, objective and camera assembly along the

optical (z) axis, and by recording and digitally stacking the 2D fluorescence patterns at linearly spaced depths. A NI-DAQ (National Instruments, NI PCIe-6363) synthesizes custom analog signals to synchronously modulate the lasers and the galvo-mirrors, as well as digital triggers to flip frames on the DMD. An analog input channel enabling synchronous measurements of neural photocurrent and spikes in direct response to the custom 3D light sculpting sequence. A customized MATLAB (MathWorks, U.S.) graphic user interface is used to control the NI DAQ boards, calibrate and align the photostimulation and imaging modalities, and for data acquisition and processing.

Computational reconstruction framework.

3D-MAP projects N foci simultaneously in a 3D volume (V voxels), which is defined as a stimulation pattern (i^{th} pattern A_i). The positions of the N foci are randomly selected from the V voxels. The electrophysiology readout (excitatory postsynaptic currents, EPSCs; or inhibitory postsynaptic currents, IPSCs) under this pattern is recorded and the maximum value of the EPSCs or IPSCs is the measurement y_i under the illumination of ith pattern. Thus, the forward model of multi-site simultaneous illumination is (Fig. 6a):

$$y_i = \sum_{j=1}^{V} A_{i,j} x_j,\ i = 1, 2, \ldots, P.$$

P is the number of patterns and all patterns are orthogonal to each other. To solve the synaptic connection map at the jth voxel (x_j), the number of P should be equal to V. The reconstruction framework can be formulated as a l_1- regularized optimization problem that seeks to estimate $\boldsymbol{x}$ by minimizing the difference between the measured currents ($\boldsymbol{y}$) and those expected via the forward model (Fig. 6b):

$$\underset{x \geq 0}{\operatorname{argmin}}(\|\boldsymbol{Ax} - \boldsymbol{y}\|_2^2 - \lambda R(\boldsymbol{x})),$$

where $R(\boldsymbol{x})$ describes total-variation (TV) regularization defined as

$$R(\boldsymbol{x}) = \sum_{j=1}^{V} |x_{j+1} - x_j|.$$

This optimization problem is solved using fast iterative shrinkage-thresholding algorithm (FISTA), which is a first-order gradient descent algorithm. FISTA is able to reconstruct the result (Fig. 6c-d, Fig. S3) in real time during the experiments. The algorithm is summarized in Algorithm 1.

Algorithm 1. 3D-MAP algorithm

---

1. **Procedure** 3D-MAP multi-sites mapping reconstruction
2. Initialize $\boldsymbol{x}_0$ by uniformly distributed random numbers between [0 1]
3. $k \leftarrow 0$
4. **while** $k < maxiter$ **do**
    a. Gradient $\Delta\boldsymbol{x} \leftarrow FISTA[\boldsymbol{x}_0, \boldsymbol{A}, \boldsymbol{y}, \lambda]$
    b. $\boldsymbol{x}_{k+1} = \boldsymbol{x}_k - \mu\Delta\boldsymbol{x}_k$, where μ is the step size
    c. $k = k + 1$
5. **return** $\boldsymbol{x}$

If every voxel is illuminated M times (the number of repetitions) using P patterns and each pattern illuminates N voxels, we can draw the relation between these parameters:

$$P = MV/N.$$

To solve $\boldsymbol{x}$, P should be equal to V, that is, the number of repetitions (M) should equal to the number of foci (N). However, the number of repetitions could be smaller than M if the multiple illumination foci satisfy these two assumptions: first, the foci are distributed sparsely in the volume; second, the readout postsynaptic current is a linear combination of the response from presynaptic neurons stimulated by these foci. As shown in Fig. S3,

where the number of foci is five (N=5), it is possible to reconstruct the synaptic connection map coarsely with less than five repetitions (M=1-4).

Animal preparation and electrophysiology

Neonatal mice age P3-P4 (wild type, emx1-IRES-Cre (JAX stock#005628), or emx1-Cre;GAD67-GFP (MGI:3590301)) were cryoanesthetized on ice and mounted in a head mold. AAVs driving Cre-dependent expression of either soma-targeted ChroME (Fig. 4-5, Fig. S2-3) or Chrimson (Fig. 6) were injected via a Nanoject3 (Drummond) into the visual cortex (~1-2 mm lateral to lambda, 3 sites, 22 nL/ site), ~100-300 microns below the brain surface. In wild type mice we injected AAV-mDlx-ChroME to drive opsin expression in cortical interneurons. All expression vectors co-expressed nuclear targeted mRuby3. Mice were used for brain slice or *in vivo* recordings at P28-P56. Brain slices were prepared as previously described[22]. Slices were transferred to a chamber and perfused with ACSF (no receptor blockers) warmed to ~33 degrees Celsius. First the microscope objective was centered over the area of V1 with the highest expression density of the opsin, as indicated by the density of mRuby3-expressing cells. ACSF contained in mM: NaCl 119, KCl 2.5, $MgSO_4$ 1.3, $NaH_2PO_4$1.3, glucose 20, $NaHCO_3$ 26, $CaCl_2$ 2.5. Internal solutions contained $CsMeSO_4$ (for voltage clamp) or KGluconate (for current clamp) 135 mM and NaCl 8 mM, HEPES 10 mM, Na_3GTP 0.3 mM, MgATP 4 mM, EGTA 0.3 mM, QX-314-Cl 5 mM (voltage clamp only), TEA-Cl 5mM (voltage clamp only). For loose-patch experiments pipettes were filled with ACSF. The resistance of the patch electrodes ranged from 3-5 megaohms. For direct recording of photocurrents or light induced spiking, we patched neurons (either in loose patch or whole cell patch clamp) that expressed mRuby3. For recording light-driven synaptic inputs we patched

from unlabeled putative interneurons (that did not have pyramidal morphology), or from GFP-expressing neurons in GAD67-GFP mice.

For optogenetic mapping we generated light spots ~10 microns wide (apertures of 10-20 pixels in radius on DMD). The total stimulation duration was 3-6 milliseconds. For ChroME-expressing animals we used 473 nm light (Fig. 3a-e, Fig. 4-5, Fig. S2-3), and for Chrimson we used 635 nm light (Fig. 6). All mapping used fully randomized sequences. For measurement of PPSFs and multi-spot synaptic maps we used the system in full 3D mode (Fig. 3, Fig. 5-6, Fig. S3). For single spot synaptic maps all photo-stimuli were at the native focal plane, and the microscope was moved mechanically under software control to obtain input maps at different axial planes (Fig. 4, Fig. S2). Mapping at the native focal plane requires only one DMD mask per light stimulus as compared to ten for a full 3D pattern, allowing for many more masks to be stored in the DMD RAM and rapidly displayed. Galvo-mirrors scans continuously in 2π to enable z-section when mapping at the native focal plane, which is different from direct 2D projection. At the beginning of each mapping experiment we first took a ten-point laser-power dose response curve of the photocurrent or light-induced synaptic current and used this data to choose the power range for photocurrent or synaptic mapping. For spiking PPSFs, the lowest light level that reliably generated spikes when directly targeting the soma was used. For single spot mapping we updated the DMD pattern at 40-80 Hz. For multi-spot mapping we updated the DMD pattern at 10-20 Hz, which minimized network adaptation.

For *in vivo* recording, mice were sedated with chlorprothixene (0.075 mg) and anesthetized with isoflurane (1.5-2%). A small stainless steel plate was attached to the skull with Metabond. The skull was protected with cyanoacrylate glue and dental cement (Orthojet). A 2.5 mm craniotomy was made over V1 with a circular biopsy punch. The dura was removed with fine forceps and the craniotomy was covered with 1.2% agarose in ACSF and additional ACSF. The mouse was then injected with urethane for prolonged anesthesia (0.04 g), and supplemented with 0.5-1.5% isoflurane at the recording rig. Body temperature was maintained at 35-37 degrees Celsius with a warming blanket. Neurons were recorded under visualization either with epifluorescence (to target opsin expressing neurons in the upper 100 microns of the brain for PPSF measurements) or in L2/3 via oblique infrared contrast imaging via an optic fiber (200 microns diameter) placed at a ~25 degree angle from horizontal located as close as possible to the brain surface underneath the objective. The same procedure for optogenetic mapping used *in vitro* was used *in vivo*. All data analysis was performed in MATLAB.

Acknowledgements: This work was supported by DARPA N66001-17-C-40154 to H.A. and L.W., as well as NIH UF1NS107574 to H.A. and L.W. This work was supported by the New York Stem Cell Foundation. H.A. is a New York Stem Cell Foundation Robertson Investigator. This work was funded by the Gordon and Betty Moore Foundation's Data-Driven Discovery Initiative through Grant GBMF4562 to L.W. This work was also funded by Burroughs Wellcome Fund, Career Award at the Scientific Interface to N.P..

Author contributions

All authors contributed to the development of 3D-MAP. N.P. developed the pilot version of 3D-MAP and the algorithm of 3D image synthesis. Y.X. designed and assembled the current experimental setup, performed simulation and experimental measurements for the optical characterization of the PSF, developed the optimization reconstruction algorithm, and performed data processing in all sections. H.A. designed and performed electrophysiology experiments in mouse brain slice and in anesthetized mouse and advised the research. Y.X. and H.A. wrote the manuscript with additional input form N.P and L.W.. L.W. helped advise Y.X. and N.P.

References

1. Deisseroth, K. Optogenetics. *Nat. Methods* **8**, 26–29 (2011).
2. Zhang, F. *et al.* Multimodal fast optical interrogation of neural circuitry. *Nature* **446**, 633–639 (2007).
3. Adam, Y. *et al.* Voltage imaging and optogenetics reveal behaviour-dependent changes in hippocampal dynamics. *Nature* **569**, 413–417 (2019).
4. Szabo, V., Ventalon, C., De Sars, V., Bradley, J. & Emiliani, V. Spatially selective holographic photoactivation and functional fluorescence imaging in freely behaving mice with a fiberscope. *Neuron* **84**, 1157–1169 (2014).
5. Carrillo-Reid, L., Han, S., Yang, W., Akrouh, A. & Yuste, R. Controlling Visually Guided Behavior by Holographic Recalling of Cortical Ensembles. *Cell* **178**, 447–457.e5 (2019).
6. Sohal, V. S., Zhang, F., Yizhar, O. & Deisseroth, K. Parvalbumin neurons and gamma rhythms enhance cortical circuit performance. *Nature* **459**, 698–702 (2009).
7. Liu, X. *et al.* Optogenetic stimulation of a hippocampal engram activates fear memory recall. *Nature* **484**, 381–385 (2012).
8. Naka, A. *et al.* Complementary networks of cortical somatostatin interneurons enforce layer specific control. *Elife* **8**, (2019).

9. Anselmi, F., Ventalon, C., Bègue, A., Ogden, D. & Emiliani, V. Three-dimensional imaging and photostimulation by remote-focusing and holographic light patterning. *Proc. Natl. Acad. Sci. U. S. A.* **108**, 19504–19509 (2011).
10. Werley, C. A., Chien, M.-P. & Cohen, A. E. Ultrawidefield microscope for high-speed fluorescence imaging and targeted optogenetic stimulation. *Biomed. Opt. Express* **8**, 5794–5813 (2017)
11. Sakai, S., Ueno, K., Ishizuka, T. & Yawo, H. Parallel and patterned optogenetic manipulation of neurons in the brain slice using a DMD-based projector. *Neurosci. Res.* **75**, 59–64 (2013).
12. Nikolenko, V. *et al.* SLM Microscopy: Scanless Two-Photon Imaging and Photostimulation with Spatial Light Modulators. *Front. Neural Circuits* **2**, 5 (2008).
13. Papagiakoumou, E. *et al.* Scanless two-photon excitation of channelrhodopsin-2. *Nat. Methods* **7**, 848–854 (2010).
14. Pégard, N. C. *et al.* Three-dimensional scanless holographic optogenetics with temporal focusing (3D-SHOT). *Nat. Commun.* **8**, 1228 (2017).
15. Mardinly, A. R. *et al.* Precise multimodal optical control of neural ensemble activity. *Nat. Neurosci.* **21**, 881–893 (2018).
16. Picot, A. *et al.* Temperature Rise under Two-Photon Optogenetic Brain Stimulation. *Cell Rep.* **24**, 1243–1253.e5 (2018).
17. Sun, S., Zhang, G., Cheng, Z., Gan, W. & Cui, M. Large-scale femtosecond holography for near simultaneous optogenetic neural modulation. *Opt. Express* **27**, 32228–32234 (2019).
18. de Groot, A. *et al.* NINscope, a versatile miniscope for multi-region circuit investigations. *Elife* **9**, (2020).
19. Xue, Y. *et al.* Scanless volumetric imaging by selective access multifocal multiphoton microscopy. *Optica* vol. 6 76 (2019).
20. Zhang, J., Pégard, N., Zhong, J., Adesnik, H. & Waller, L. 3D computer-generated holography by non-convex optimization. *Optica, OPTICA* **4**, 1306–1313 (2017).
21. Prevedel, R. *et al.* Fast volumetric calcium imaging across multiple cortical layers using sculpted light. *Nat. Methods* (2016).
22. Pluta, S. *et al.* A direct translaminar inhibitory circuit tunes cortical output. *Nat. Neurosci.* **18**, 1631–1640 (2015).

Supplementary figures

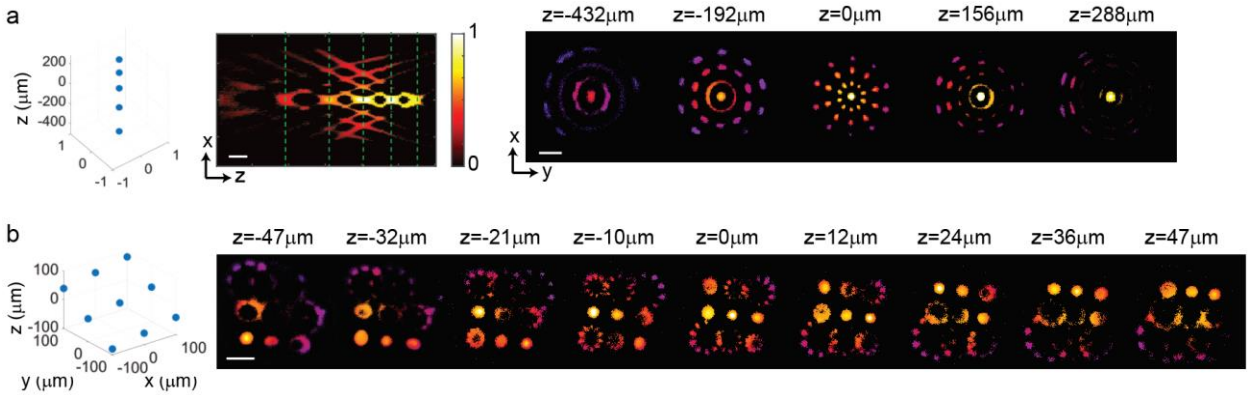

Fig. S1. 3D-MAP is able to simultaneously generate multiple foci located anywhere in 3D. (a) Five foci are located right on top of each other along the z-axis. Left: XZ cross-section. Right: XY cross-section corresponding to the z depths marked with green dash lines. (b) Nine foci located in a 3D volume and each of them lying on a different plane. For both (a) and (b), the target location is indicated in the 3D diagram on the left, and the corresponding experimental 3D fluorescence measurements are on the right. The foci are recorded in 3D by capturing a stack of 2D fluorescence images at various depths of the 3D illumination pattern intercepting a thin, uniform, fluorescent calibration slide with a sub-stage objective coupled to a camera. Scale bar, 100μm.

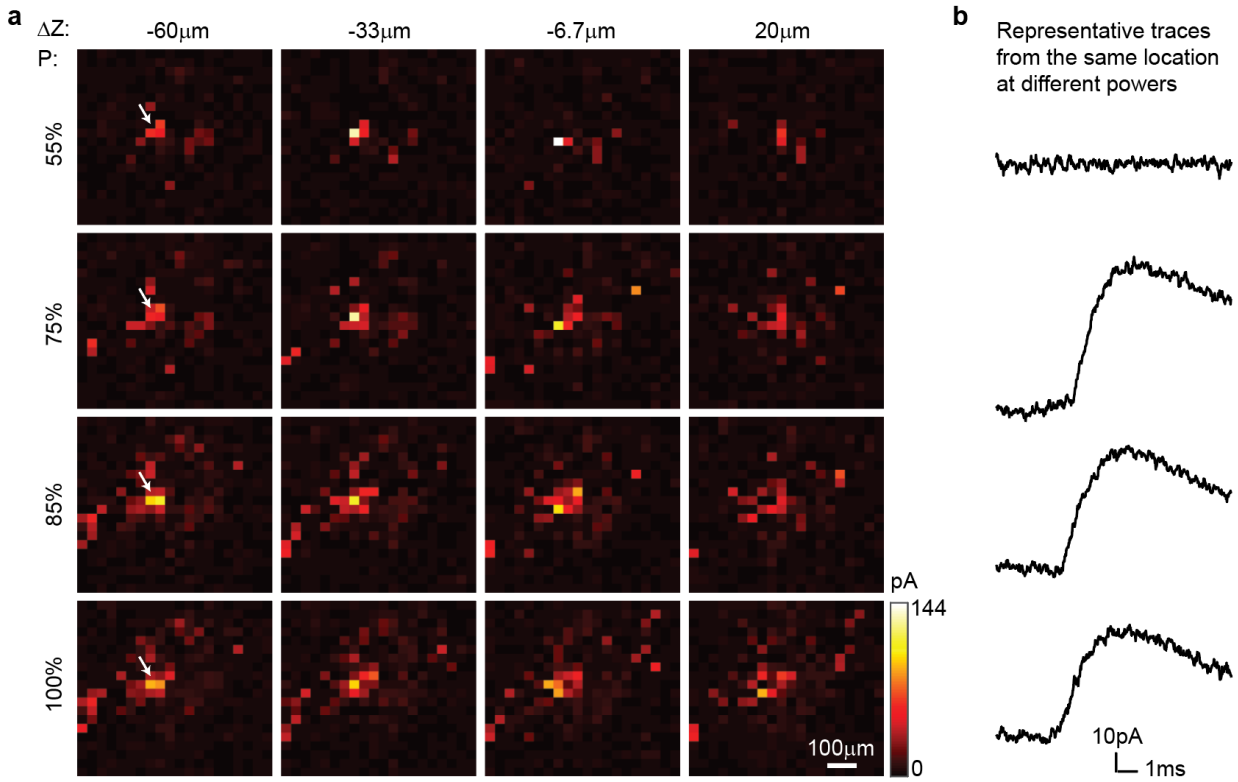

Fig. S2. 3D-MAP provides mapping of inhibitory synaptic connections *in vivo*. We patched a pyramidal neuron without opsin and photo-stimulated the volume around it pixel-by-pixel while the parvalbumin neurons connecting to this patched cell via synapses expressed opsin. The current readout reveals the inhibitory synaptic connections from all parvalbumin neurons to this pyramidal neuron. The mapping process is repeated 4 times. (a) Each row of the images is measured under the same stimulation laser power (100% power is 419μW), and each column of the images is at the same axial plane. Scale bar: 100μm. (b) Representative traces of postsynaptic currents under each stimulation power (measured from the pixel pointed by white arrow). These traces elucidate the synaptic connection is binary: once the neuron is photo-stimulated, the synaptic current remains the same, even if the stimulation power

is increased. The unique photosensitivity of each neuron helps us to identify different neural ensembles by changing the stimulation power.

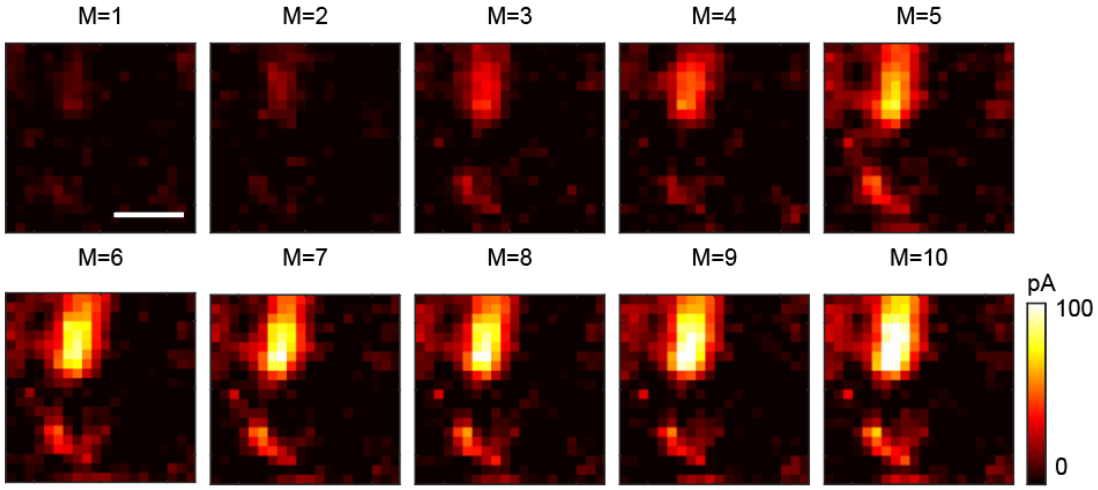

Fig. S3. Multi-site simultaneous stimulation by 3D-MAP can reconstruct synaptic connectivity maps with fewer measurements than single-target stimulation. M: number of repeat measurements (see Methods). The data is recorded from five foci simultaneously stimulated. When M is less than five, the optimization problem is underdetermined. Assuming the five foci stimulate sites which are sparsely distributed in space, it is possible to reconstruct the synaptic connectivity map with fewer measurements (M=1-4) using compressive sensing. Scale bar, 100μm.